Mitochondrial dysfunction and reduced prostaglandin synthesis in skeletal muscle of Group VIB Ca^{2+}-independent phospholipase $A_2\gamma$-deficient mice[S]

Emiko Yoda,* Keiko Hachisu,* Yoshitaka Taketomi,*,§ Kotomi Yoshida,* Masanori Nakamura,† Kazutaka Ikeda, Ryo Taguchi,** Yoshihito Nakatani,* Hiroshi Kuwata,* Makoto Murakami,*,§ Ichiro Kudo,[1],* and Shuntaro Hara[2],***

Department of Health Chemistry,* School of Pharmaceutical Sciences and Department of Oral Anatomy and Developmental Biology,† School of Dentistry, Showa University, Tokyo, Japan; Tokyo Metropolitan Institute of Medical Science,§ Tokyo, Japan; Department of Metabolome,** Graduate School of Medicine, University of Tokyo, Tokyo, Japan

Abstract Group VIB Ca^{2+}-independent phospholipase $A_2\gamma$ ($iPLA_2\gamma$) is a membrane-bound $iPLA_2$ enzyme with unique features, such as the utilization of distinct translation initiation sites and the presence of mitochondrial and peroxisomal localization signals. Here we investigated the physiological functions of $iPLA_2\gamma$ by disrupting its gene in mice. $iPLA_2\gamma$-knockout (KO) mice were born with an expected Mendelian ratio and appeared normal and healthy at the age of one month but began to show growth retardation from the age of two months as well as kyphosis and significant muscle weakness at the age of four months. Electron microscopy revealed swelling and reduced numbers of mitochondria and atrophy of myofilaments in $iPLA_2\gamma$-KO skeletal muscles. Increased lipid peroxidation and the induction of several oxidative stress-related genes were also found in the $iPLA_2\gamma$-KO muscles. These results provide evidence that impairment of $iPLA_2\gamma$ causes mitochondrial dysfunction and increased oxidative stress, leading to the loss of skeletal muscle structure and function. We further found that the compositions of cardiolipin and other phospholipid subclasses were altered and that the levels of myoprotective prostanoids were reduced in $iPLA_2\gamma$-KO skeletal muscle. Thus, in addition to maintenance of homeostasis of the mitochondrial membrane, $iPLA_2\gamma$ may contribute to modulation of lipid mediator production in vivo.—Yoda, E., K. Hachisu, Y. Taketomi, K. Yoshida, M. Nakamura, K. Ikeda, R. Taguchi, Y. Nakatani, H. Kuwata, M. Murakami, I. Kudo, and S. Hara. **Mitochondrial dysfunction and reduced prostaglandin synthesis in skeletal muscle of Group VIB Ca^{2+}-independent phospholipase A2γ-deficient mice. *J. Lipid Res.* 2010.** 51: **3003–3015.**

Supplementary key words cardiolipin • mitochondria • muscle • phospholipids

Phospholipase A_2 (PLA_2) enzymes catalyze the cleavage of the *sn*-2 ester bond of glycerophospholipids to yield free fatty acids and lysophospholipids, thereby playing critical roles in cellular lipid metabolisms linked to energy storage, membrane remodeling, and lipid mediator signaling. In the membrane remodeling reaction, fatty acyl groups are first removed (deacylated) by PLA_2 and then replaced (reacylated) with different fatty acyl groups by acyltransferases, which allow membrane phospholipids to acquire a variation of molecular species. In the signaling reaction, polyunsaturated fatty acids [typically arachidonic acid (AA)] and lysophospholipids released by the action of PLA_2s are metabolized to various lipid mediators, such as prostaglandins (PG), leukotrienes, and platelet-activating factor, which exert a variety of biological actions through their cognate receptors.

This work was supported by a Showa University special grant-in-aid for Innovative Collaborative Research Projects and grants-in-aid for Scientific Research and High-Tech Research Center Project for Private Universities, with a matching fund subsidy (2004–2007) from the Japanese Ministry of Education, Science, Culture, Sports and Technology. M. Murakami was also supported by Precursory Research for Embryonic Science and Technology (PRESTO) of the Japan Science and Technology Agency.

Manuscript received 28 April 2010 and in revised form 12 July 2010.

Published, JLR Papers in Press, July 12, 2010
DOI 10.1194/jlr.M008060

Abbreviations: AA, arachidonic acid; CL, cardiolipin; COX, cyclooxygenase; CT, computed tomography; GPx, glutathione peroxidase; HBSS, Hank's balanced salt solution; HO, heme oxigenase; HS, horse serum; KO, knockout; MDA, malondialdehyde; MT, methallothionein; Nqo, NAD(P)H dehydrogenase, quinine; PAF, platelet-activating factor; PC, phosphatidylcholine; PE, phosphatidylethanolamine; PG, prostaglandin; PGD_2, prostaglandin D_2; PGE_2, prostaglandin E_2; $PGF_{2\alpha}$, prostaglandin $F_{2\alpha}$; PGI_2, prostaglandin I_2; PLA_2, phospholipase A_2; $cPLA_2$, cytosolic PLA_2; $iPLA_2$, calcium-independent PLA_2; $sPLA_2$, secretory PLA_2; Q-PCR, quantitative RT-PCR; ROS, reactive oxygen species; SOD, superoxide dismutase; TXA_2, thromboxane A_2; WT, wild-type.

[1] Deceased.
[2] To whom correspondence should be addressed.
e-mail: haras@pharm.showa-u.ac.jp

[S] The online version of this article (available at http://www.jlr.org) contains supplementary data in the form of four figures and four videos.

PLA_2 enzymes have been classified into five major families: secretory PLA_2 ($sPLA_2$), cytosolic PLA_2 ($cPLA_2$), Ca^{2+}-independent PLA_2 ($iPLA_2$), platelet-activating factor acetylhydrolase, and lysosomal PLA_2, each of which occurs as multiple isoforms (1–3). Among these, the $cPLA_2$ and $iPLA_2$ families represent intracellular enzymes with a catalytic serine in their lipase consensus motif and are thought to diverge from a common ancestral gene (3). Currently, nine members of the $iPLA_2$ family, also referred to as the patatin-like phospholipase-domain-containing family, have been identified. These $iPLA_2$ isoforms share sensitivity to 4-bromoenol lactone, a mechanism-based irreversible inhibitor (4). Among them, two abundant isoforms of $iPLA_2$ are thought to play important roles in the deacylation of cellular phospholipids. The first one is group VIA $iPLA_2$ (also called $iPLA_2\beta$) (5, 6), which was initially assumed to be the housekeeping enzyme responsible for phospholipid acyl group turnover and generation of the lysophospholipids necessary for AA incorporation (7). Subsequent studies employing $iPLA_2\beta$-knockdown cells and knockout (KO) mice have provided evidence that $iPLA_2\beta$ plays roles not only in phospholipid homeostasis but also in signaling in diverse biological events (8–16). The second isoform of $iPLA_2$, group VIB $iPLA_2$ (also called $iPLA_2\gamma$), was identified by a search of the expressed sequence tag database for sequences homologous to $iPLA_2\beta$. The gene for $iPLA_2\gamma$ encodes a full-length 88 kDa protein, yet it can also be transcribed to N-terminally truncated 63, 74, and 77 kDa forms due to the utilization of distinct translation initiation sites (17). $iPLA_2\gamma$ has been reported to be localized in mitochondria, peroxisomes, and the endoplasmic reticulum. Because of this localization in organelles related to fatty acid β-oxidation and synthesis, $iPLA_2\gamma$ has been postulated to participate in the homeostatic lipid catabolism and turnover linked to bioenergic processes.

Recent gene-targeting studies of $iPLA_2\gamma$ have unveiled a particular role of this enzyme in the metabolism of cardiolipin (CL), a critical mitochondrial phospholipid that facilitates protein supercomplex formation in the mitochondrial inner membrane, thereby allowing optimal electron transport chain function (18, 19). Genetic ablation of $iPLA_2\gamma$ resulted in the generation of viable progeny that demonstrated decreased growth, cold intolerance due to impaired fat burning in brown adipose tissue, and defects in ascorbate-stimulated mitochondrial Complex IV function in the myocardium (18). Furthermore, these knockout mice also showed alterations in hippocampal CL content, mitochondrial degeneration, and cognitive dysfunction (19). These reports suggest that $iPLA_2\gamma$, a mitochondrial $iPLA_2$, regulates mitochondrial inner membrane lipid metabolism, perturbation of which may profoundly influence fatty acid β-oxidation, oxygen consumption, energy expenditure, and thus, tissue homeostasis.

In addition to its bioenergetic functions, the signaling role of $iPLA_2\gamma$ has been revealed by several in vitro studies. For instance, overexpression of $iPLA_2\gamma$ has been shown to promote spontaneous and agonist-stimulated release of AA, which is converted to PGE_2 with preferred cyclooxygenase (COX)-1 coupling in HEK293 cells (20). The induction of group IIA $sPLA_2$ by pro-inflammatory stimuli has been shown to require $iPLA_2\gamma$ through production of certain lipid metabolite(s) in rat fibroblastic 3Y1 cells (21). In addition, $iPLA_2\gamma$ could produce 2-arachidonoyl-lysphosphatidylcholine, a presumptive lipid mediator, through its PLA_1 action (22). Although these observations suggest that $iPLA_2\gamma$ is able not only to regulate the remodeling of lipid membranes but also to modify the production of lipid mediator(s), no in vivo evidences for its role in such a signaling process have been obtained.

In this study, we established an additional line of $iPLA_2\gamma$-deficient mice and found that the mice showed growth retardation and reduced exercise capacity, which had also been demonstrated for the initial line of null mice (18, 19). We found that this phenotype was caused by skeletal muscle atrophy. Analysis of the skeletal muscle showed decreased mitochondrial number, markedly enlarged and swollen mitochondria, and mitochondrial dysfunction accompanied by increasing oxidative stress in $iPLA_2\gamma$-deficient mice. We further found that the compositions of CL and other phospholipid subclasses were altered, and the levels of $PGF_{2\alpha}$ and PGD_2 were reduced in $iPLA_2\gamma$-knockout skeletal muscle. Therefore, in addition to its maintenance of homeostasis of the mitochondrial membrane, $iPLA_2\gamma$ may also contribute to modulation of lipid mediator production in vivo.

EXPERIMENTAL PROCEDURES

Materials

Collagenase type II was obtained from Worthington Biochemicals (Lakewood, NJ). Fetal calf serum (FCS) and horse serum (HS) were obtained from Bioserum (Middlesex, UK). Hank's balanced salt solution (HBSS), basic fibroblast growth factor, penicillin-streptomycin solution and HamF10 medium were obtained from Gibco/Invitrogen (Grand Island, NY). Dulbecco's modified Eagle's medium (DMEM) was obtained from Nissui Pharmaceutical (Tokyo, Japan). Rabbit polyclonal antibody against rat cytosolic PGE synthase (cPGES; p23) and rabbit polyclonal antibody against human $iPLA_2\gamma$ were prepared as described previously (21, 23). Mouse monoclonal antibody against human α-tubulin and horseradish peroxidase-conjugated anti-IgG antibodies were purchased from Zymed Laboratories. (South San Francisco, CA). Rabbit polyclonal antibody against human manganese superoxide dismutase (MnSOD/SOD2) and goat polyclonal antibody against human F_1-ATPase were purchased from Santa Cruz Biotechnology (Santa Cruz, CA). Rabbit polyclonal antibodies against chicken α-actinin and indomethacin were purchased from Sigma Chemical (St. Louis, MO). Mouse monoclonal antibody against human porin and mouse skeletal muscle C2C12 myoblast cells were obtained from Prof. M. Shibanuma (Showa University, Tokyo, Japan), and the cells were maintained in DMEM with 10% FCS. All other reagents were from Sigma Chemical.

Mice

$iPLA_2\gamma$-KO mice were produced by and obtained from TransGenic, Inc. (Kumamoto, Japan). The $iPLA_2\gamma$ gene was disrupted by gene-trapping methods (24), in which a gene cassette consisting of a splicing acceptor (SA)-βgeo-pA-pSP73 was integrated between exons 1 and 2 (supplementary Fig. IA). The SA contains

three stop codons inframed with the ATG of the β-galactosidase/neomycin-resistance fusion gene (βgeo), which can function in promoter trapping. These mice were further backcrossed 10 generations onto a C57BL/6 background. All mice were housed in climate-controlled (21°C), specific pathogen-free facilities with a 12 h light/dark cycle, with free access to standard laboratory food (Picolab mouse diet 20; Laboratory Diet, Brentwood, MO) and water. All procedures involving animals were performed under approved institutional guidance. The genotypes of $iPLA_2\gamma^{+/+}$ and $iPLA_2\gamma^{-/-}$ were confirmed by polymerase chain reaction (PCR) using tail DNA as a template and a set of the sense primer 5′-CCGTGACTACTGCCTGCGT-3′ and the antisense-1 primer 5′-CAAGCGATTGGGAGTGAGTTGG-3′, which amplified a 1409-bp fragment in $iPLA_2\gamma^{+/+}$ wild-type (WT) mice, or a set of the sense primer and the antisense-2 primer 5′-CTGGAGAAGGC-CCGACCATC-3′, which amplified a 745-bp fragment in $iPLA_2\gamma^{-/-}$ mice.

Computed tomography analysis

Muscle volume was analyzed in the four-month-old WT and $iPLA_2\gamma$-KO mice using computed tomography (CT) systems (eXplore Locus; GE Healthcare, London, ON, Canada). Mice were anesthetized with 2% isoflurane (Dainippon Sumitomo Pharmaceutical Co. Ltd., Osaka, Japan) and scanned for 10 min under the following conditions: resolving power, 93 μm; view number, 400; voltage, 80 kVp; and electric current, 450 μA. CT images were analyzed using MicroView 2.0 software (GE Healthcare). For microCT analysis, mice were kept in a lateral position on a microCT SM90-CT (Shimadzu Co., Kyoto, Japan). The angles of spine curvature were determined by TRI/3D-BON software.

SDS-PAGE and Western blotting

Tissue homogenates or cell lysates (10 μg protein equivalents) were subjected to SDS-PAGE using 7.5% or 12% gels under reducing conditions. The separated proteins were electroblotted onto nitrocellulose membranes (Schleicher and Schuell, Keene, NH) with a semidry blotter (Bio-Rad Laboratories, Hercules, CA) according to the manufacturer's instructions. After blocking with 5% (w/v) skim milk in 10 mM Tris-HCl, pH 7.4, containing 150 mM NaCl and 0.05% Tween 20, the membranes were probed with the respective antibodies (1:5,000 dilution) for 2 h, followed by incubation with horseradish peroxidase-conjugated anti-mouse (1:5,000 for α-tubulin and porin), anti-rabbit (1:5,000 for SOD2, $iPLA_2\gamma$, cPGES, and α-actinin), or anti-goat (1:10,000 for F_1-ATPase) IgG. After being washed, the membranes were visualized with Western Lightning Chemiluminescence Reagent Plus (Perkin Elmer Life Sciences, Boston, MA) as described previously (21).

Histology

For transmission electron microscopy, skeletal muscle tissue was fixed with 2.5% glutaraldehyde for 16 h at 4°C, postfixed with 2% OsO_4 for 2 h at 4°C, dehydrated by an ascending ethanol series, passed through propylene oxide, and then embedded in Quetol812 resin (Nisshin EM, Tokyo, Japan). Ultrathin sections (90 nm thick) on mesh grids were stained with uranyl acetate and lead acetate and examined with an H-300 electron microscope (Hitachi, Tokyo, Japan). For histopathology, tissue sections were fixed in 10% formalin, embedded in paraffin, and stained with hematoxylin-eosin by a standard method. These paraffin sections were then additionally stained with Masson trichrome and Victoria blue (Wako) to examine the degree of organization and the fibrosis. Finally, the sections were stained with TUNEL to detect degenerating cells according to the manufacturer's instructions (Apoptag Plus Peroxidase In Situ Apoptosis Detection Kit; Chemicon International, Temecula, CA).

Primary myocytes culture

Primary myocytes were cultured from fore- and hindlimbs of $iPLA_2\gamma$-KO and WT mice. The skeletal muscle was excised, minced, and then incubated at 37°C for 30 min with 2 ml of HBSS containing 0.2% (w/v) collagenase type II in HBSS per gram of tissue. Collagenase digestion was halted by the addition of ice-cold phosphate-buffered saline (PBS). The tissue slurry was then strained through a 100-μm filter and then a 40-μm filter (Becton Dickinson, Bedford, MA) and centrifuged at 500 *g* for 5 min. The pellet was resuspended in hypotonic solution [0.83% (w/v) NH_4Cl: 0.17 M Tris-HCl pH 7.65 = 9:1], and after the reaction was stopped by the addition of PBS, it was centrifuged at 500 *g* for 5 min. The pellet was resuspended in growth medium (HamF10 medium containing 20% FCS, 2.5 ng/ml basic fibroblast growth factor, and 100 U/ml penicillin/100 μg/ml streptomycin), and the cells were plated in plastic dishes overnight at 37°C under 5% CO_2. The unattached cells were seeded in collagen type-I-coated dishes (Iwaki Glass, Tokyo, Japan). The medium was changed every 2–3 days. After 1 or 2 weeks, when the adhering cells reached 70–80% confluence, they were dispersed by trypsinization and plated on collagen type-I-coated dishes in growth medium. After 2 or 3 days, myoblast fusion was induced by shifting the cells to a differentiation medium (DMEM supplemented with 5% HS and 100 U/ml penicillin/100 μg/ml streptomycin) for 3–6 days.

Behavioral testing

Each animal's grip was monitored by the wire hang test, also known as the wire-mesh test (13). The animals were placed on lattice covers held horizontally. The covers were first turned upright for 20 s and then upside down for an additional 120 s. Each animal was individually tested in two trials. The time at which the animal lost its grip was recorded.

Knockdown of $iPLA_2\gamma$

siRNAs [Silencer predesigned siRNA $iPLA_2\gamma$-specific (ID #295428) and Silencer control siRNA (Applied Biosystems, Cambridge, MA)] were transfected into C2C12 cells with LipofectamineTM RNAiMAX Reagent (Invitrogen Life Technologies, Carlsbad, CA) according to the manufacturer's instructions. Three days after transfection, the cells were used for the analyses.

Determination of tissue ATP content

Tissue or cell ATP content was determined using an ATP assay kit of tissues (TOYO Ink Co., Tokyo, Japan). Briefly, tissue pieces (100 mg) or cell lysate were homogenized in 10 ml homogenate buffer (0.25 M sucrose in 10 mM HEPES-NaOH, pH 7.4) and centrifuged at 1,000 *g* at 4°C for 10 min. Then 700 μl of homogenate buffer was added to 100 μl of the upper phase after the extraction of ATP and assayed using the ATP assay kit.

Quantitative RT-PCR

Total RNA was extracted from the thigh muscles of four-month-old WT and KO mice (n = 7) with TRIzol reagent (Invitrogen). First-strand cDNA synthesis was conducted by using a High Capacity cDNA Reverse Transcription Kit (Applied Biosystems, Foster City, CA) according to the manufacturer's instructions. Then 100 ng of synthesized cDNA was used as a template for the quantitative RT-PCR (Q-PCR) reactions. Q-PCR was performed using a StepOne Real-time PCR System (Applied Biosystems) with SYBR Green Reagent (Applied Biosystems) according to the manufacturer's instructions.

The primer pairs were 5′-CTCTATCGAAAGTTGGGCTCAGA-3′ and 5′-TCCCACGTGTTACTGTCATAAAAC-3′ for mouse $iPLA_2\gamma$

(*Pnpla8*); 5′-CGGACGCCTCGTCAACA-3′ and 5′-CGGAATGGGTTCGAGAACAA-3′ for mouse iPLA$_2$β (*Pnpla9*); 5′-CCCTGAGTAGTTTGAAGGAAAAGG-3′ and 5′-ACACGTGAAGAGAGGCAAAGG-3′ for mouse cPLA$_2$α (*pla2g4a*); 5′-TTCGTATTGCGCCGCTAGA-3′ and 5′-CTTTCGCTCTGGTCCGTCTT-3′ for mouse 18s rRNA (rRNA); 5′-GGTCCTCTAAGCGTCACCAC-3′ and 5′-GAGCAGTTGGGGTCCATTC-3′ for mouse metallothionein-1 (*Mt1*); 5′-GCCCGCATGCAGATCCT-3′ and 5′-GGTCTCCTCCCAGACGGTTT-3′ for mouse NAD(P)H dehydrogenase, quinone 1 (*Nqo1*); 5′-GGTGATGCTGACAGAGGAACAC-3′ and 5′–TCTGACGAAGTGACGCCATCT-3′ for mouse heme oxygenase-1 (*Hmox1*); 5′-CCTGCCTGTGTGCTTACAACTG-3′ and 5′-GGTCCCGCCCGTCACT-3′ for mouse atrogin-1 (*Fbxo32*); 5′-TTGACGGACCCCAAAAGATG-3′ and 5′-TGGACAGCCCAGGTCAAAG-3′ for mouse interleukin (IL)-1β (*Il1b*); 5′-CCACGGCCTTCCCTACTTC-3′ and 5′-TTGGGAGTGGTATCCTCTGTGA-3′ for mouse IL-6 (*Il6*); and 5′-CAGCCGATGGGTTGTACCTT-3′ and 5′-GGCAGCCTTGTCCCTTGA-3′ for mouse tumor necrosis factor (TNF)-α (*tnf*).

Lipid peroxidation assay

The quantification of malondialdehyde (MDA) was performed according to the protocol for the BIOXYTECH LPO-586 kit (Oxis International, Portland, OR). A 20–30% (w/v) homogenate of skeletal muscle or C2C12 cells was prepared in 20 mM Tris buffer, pH 7.4, containing 5 mM butylated hydroxytoluene to prevent sample oxidation. Following centrifugation at 3,000 *g* at 4°C for 10 min, the LPO-586 R1 reagent, N-methyl-2-phenylindole in 25% methanol/75% acetonitrile, was added to the supernatants, followed by the addition of 12 N HCl and incubation at 45°C for 60 min. Following centrifugation at 15,000 *g* at 4°C for 10 min, the absorbance was read at 586 nm. The protein concentration was measured using a Bio-Rad protein assay according to the manufacturer's instructions.

Thin-layer chromatography

Lipids were extracted from tissue by the method of Bligh and Dyer (25). Thin-layer chromatography (TLC) plates (Silica gel 60A; Merck KGaA, Darmstadt, Germany) were washed twice with chloroform-methanol (1:1, v/v) and activated at 120°C before use. Total lipid extracts were separated on TLC silica gel plates (20 × 20 cm, layer thickness 0.2 mm). The plates were developed with a solvent system of chloroform-methanol-acetic acid-water (85:15:10:3.5, v/v). The developed TLC plates were then stained with iodine vapor to visualize the phospholipids. After scraping the silica in bands of phosphatidylcholine (PC), phosphatidylethanolamine (PE), CL, and phosphatidylglycerol from the plates, the lipids were extracted from the silica two times by the method of Bligh and Dyer. Individual phospholipids were quantified by a molybdenum blue method (26).

Mass spectrometric analysis

Lipids were extracted from tissue by the method of Bligh and Dyer. Before lipid extraction, PC with C28:0 (14:0-14:0; m/z = 678) was added to each sample as an internal standard (2 nmol per tissue). The ESI/MS analysis was performed using a 4000Q-TRAP quadrupole-linear ion trap hybrid mass spectrometer (Applied Biosystems/MDS Sciex) with an Ultimate 3000 HPLC system (Dionex, Sunnyvale, CA) combined with an HTC PAL autosampler (CTC Analytics, Zwingen, Switzerland). The extracted lipids were subjected to ESI/MS analysis by flow injection (3 nmol phosphorus equivalent) without liquid chromatography separation. The mobile phase composition was acetonitrile/methanol/water (6:7:2, v/v/v) (plus 0.1% ammonium formate, pH 6.8) at a flow rate of 10 μl/min. The scan range of the instrument was set at m/z 200–1000 at a scan speed of 1000 Da/s. The trap fill-time was set at 1 ms in the positive ion mode. The ion spray voltage and the declustering potential were set at 5,500 V and 100 V, respectively. Nitrogen was used as the curtain gas (setting of 10 arbitrary units) and the collision gas (set to "high").

Assays for prostanoids

For measurement of prostanoids, mice were euthanized, and tissue pieces (100 mg) were homogenized with HBSS containing 10 μM indomethacin. The homogenates were adjusted to pH 3.0 with 1 N HCl, passed through Sep-Pak C18 cartridges (Waters, Milford, MA), and the retained PGs were eluted from the cartridges with 8 ml of methanol, as described previously (27). A trace amount of [^{3}H] PGE$_2$ (Cayman Chemical Co., Ann Arbor, MI) was added to the samples before passage through the cartridges to calibrate the recovery of PGs. The solvent of the samples was evaporated, and PGs were dissolved in an aliquot of buffer and assayed with commercial enzyme immunoassay kits for each prostanoid. The enzyme immunoassay kits for PGE$_2$, 6-keto-PGF$_{1\alpha}$ (a stable end product of PGI$_2$), PGF$_{2\alpha}$, PGD$_2$, and thromboxane B$_2$ (TXB$_2$) (a stable end product of TXA$_2$) were purchased from Cayman Chemical Co.

Statistics

Data were statistically evaluated by unpaired Student's *t*–test, and values of $P < 0.05$ were considered to indicate statistical significance.

RESULTS

Generation of iPLA$_2$γ-KO mice

The iPLA$_2$γ gene was disrupted as shown in supplementary Fig. IA. Mice that were homozygous for the targeted mutation (KO, iPLA$_2\gamma^{-/-}$) were generated by the intercross of heterozygous animals (iPLA$_2\gamma^{+/-}$). Among the first 527 progenies of these heterozygous crosses, 145 (27.5%) were iPLA$_2\gamma^{+/+}$, 261 (49.5%) were iPLA$_2\gamma^{+/-}$, and 120 (23%) were iPLA$_2\gamma^{-/-}$. The number of iPLA$_2\gamma^{-/-}$ animals corresponded to that expected for simple Mendelian inheritance, suggesting that the absence of iPLA$_2$γ does not adversely affect intrauterine development or perinatal survival. To determine whether the skeletal muscle contains iPLA$_2$γ and whether iPLA$_2$γ was indeed knocked out in the null mice, its mRNA expression and protein in thigh muscles isolated from WT and iPLA$_2$γ-KO mice was analyzed by Q-PCR and Western blotting, respectively. The expression of iPLA$_2$γ mRNA (supplementary Fig. IB, left) and 88 kDa (as well as minor 77 and 63 kDa) immunoreactive iPLA$_2$γ protein (supplementary Fig. IC) was detected in the muscle of WT mice but not in that of KO mice, verifying the presence of iPLA$_2$γ (mainly as mitochondrial forms, judging from the molecular masses (20, 28)) in the skeletal muscle of WT mice and its successful ablation in KO mice. Conversely, the mRNA expression levels of other intracellular PLA$_2$, cPLA$_2$α and iPLA$_2$β, were increased in iPLA$_2$γ-KO muscle (supplementary Fig. IB, middle and right).

At birth, iPLA$_2$γ-KO mice were indistinguishable from their WT littermates. However, the body weights of iPLA$_2$γ-KO male mice after 10 weeks of age and those of female mice after 4 weeks of age were significantly lower

than those of their WT littermates (supplementary Fig. ID, a and b). The weights of heterozygous iPLA$_2\gamma^{+/-}$ mice were nearly equal to those of their WT littermates. We further found that, at two months (eight weeks) of age, the body lengths of iPLA$_2\gamma$-KO mice, both male and female, were shorter than those of their WT littermates (supplementary Fig. IE, a and b). By four months of age, both male and female iPLA$_2\gamma$-KO mice showed progressive kyphosis (curvature of the upper spine) (**Fig. 1A**). Whole-body microCT analysis revealed that iPLA$_2\gamma$-KO mice exhibited a dorsal hump arising from an increased backward curvature of the spine (Fig. 1A, b and c). To quantify this morphological observation, the angles of spine curvature were determined. The angle formed in WT mice was approximately 132°, whereas it was reduced by greater than 20% in iPLA$_2\gamma$-KO mice (Fig. 1A, d and e). Furthermore, CT analysis in a face-up position revealed that iPLA$_2\gamma$-KO mice showed scoliosis (where the spine is curved from side to side) (Fig. 1B, a and b), which appeared by four weeks of age. Since kyphosis and scoliosis have often been found in mutant mice harboring bone defects (29–32), we further analyzed the bone density by microCT analysis; however, we found no obvious difference in bone volume/tissue volume (BV/TV) between WT and KO mice (Fig. 1B, c). Hence, we concluded that iPLA$_2\gamma$-KO mice were smaller in size (both weight and length) than WT mice and had severe kyphosis and scoliosis without impairment of bone development.

By the age of four months, almost all of the iPLA$_2\gamma$-KO mice showed abnormal movement of their hindlimbs. We assessed muscular strength in two different ways. First, each mouse was placed on an upside-down beaker. WT mice struggled to stay on their feet so as not to fall off the slippery beaker. In contrast, iPLA$_2\gamma$-KO mice fell sooner because they could not stay on their feet (supplementary Video I). Second, we performed a hanging wire grip test, in which each mouse was placed on a wire net that was then turned upside down, and the latency time until the animals fell was recorded twice. Although one-month-old iPLA$_2\gamma$-KO mice showed time scores indistinguishable from those of their WT littermates, the latency of iPLA$_2\gamma$-KO mice gradually decreased afterwards and showed a greatly reduced time score at the age of four months (~60% reduction relative to that of WT mice, which maintained a steady score over four months) (Fig. 1C and supplementary Video II). These findings indicate that iPLA$_2\gamma$ deficiency leads to a gradual loss of muscular strength after weaning, which appears to be a major cause of kyphosis and scoliosis.

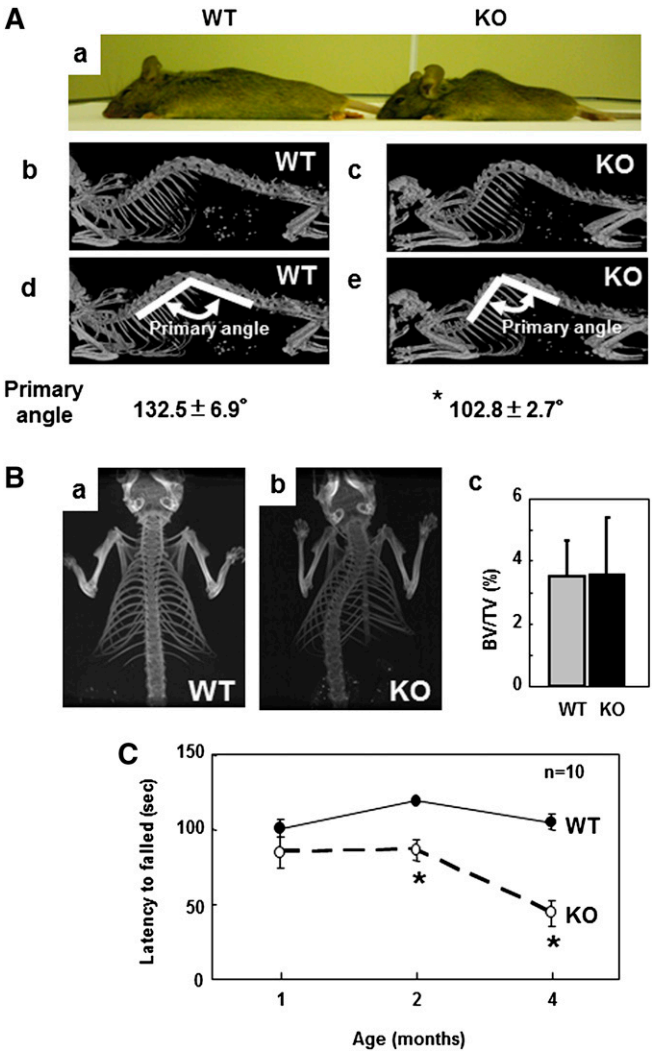

Fig. 1. Muscle weakness in iPLA$_2\gamma$-KO mice. A: Direct photography of a lateral view of WT [left (a)] and KO [right (a)] mice after anesthesia. MicroCT of a lateral view of WT [(b) and (d)] and KO [(c) and (e)] mice. In (d) and (e), the primary angles were determined at the intersection of the two lines. Quantitative data are means ± SE. * $P < 0.05$ versus WT (n = 3). B: CT scans of a face-up view of WT (a) and KO (b) mice from a dorsal side. In (c), trabecular bone volume/tissue volume (BV/TV) of WT (gray bar) and KO (black bar) mice was evaluated (n = 3). Quantitative data are means ± SE. C: Hanging wire grip test. WT (closed circles, n = 10) and KO (open circles, n = 10) mice at one , two, and four months of age were tested. Quantitative data are means ± SE. *$P < 0.001$ versus WT. Abbreviations: CT, computed tomography; iPLA$_2$, calcium-independent PLA$_2$; KO, knockout; WT, wild-type.

Muscle atrophy and mitochondrial degeneration in iPLA$_2\gamma$-deficient mice

Hematoxylin-eosin staining of the tissue sections of thigh muscles revealed some pathological characteristics in four-month-old iPLA$_2\gamma$-KO mice compared with age-matched WT mice. In the KO mice, there was wide variation in the sizes of individual fibers, with a large number of aggregated nuclei (**Fig. 2A**, a and b). The sizes of individual myofibers in iPLA$_2\gamma$-KO mice were reduced by more than 60% relative to those in WT mice, which had myofibers with a uniform size (Fig. 2B). On the other hand, at one month of age, no pathological characteristics, such as aggregated nuclei and variable sizes of muscle fibers, were observed in iPLA$_2\gamma$-KO thigh muscle sections (supplementary Fig. IIA, a and b). These results suggested that the macroscopic muscle atrophy in the KO mice proceeded from one to four months of age, and then growth retardation (supplementary Fig. ID, E) and muscle weakness (Fig. 1C) became evident. In agreement with this idea, the volumes of the thigh and leg muscles, as evaluated by axial CT analysis, were smaller in four-month-old iPLA$_2\gamma$-KO

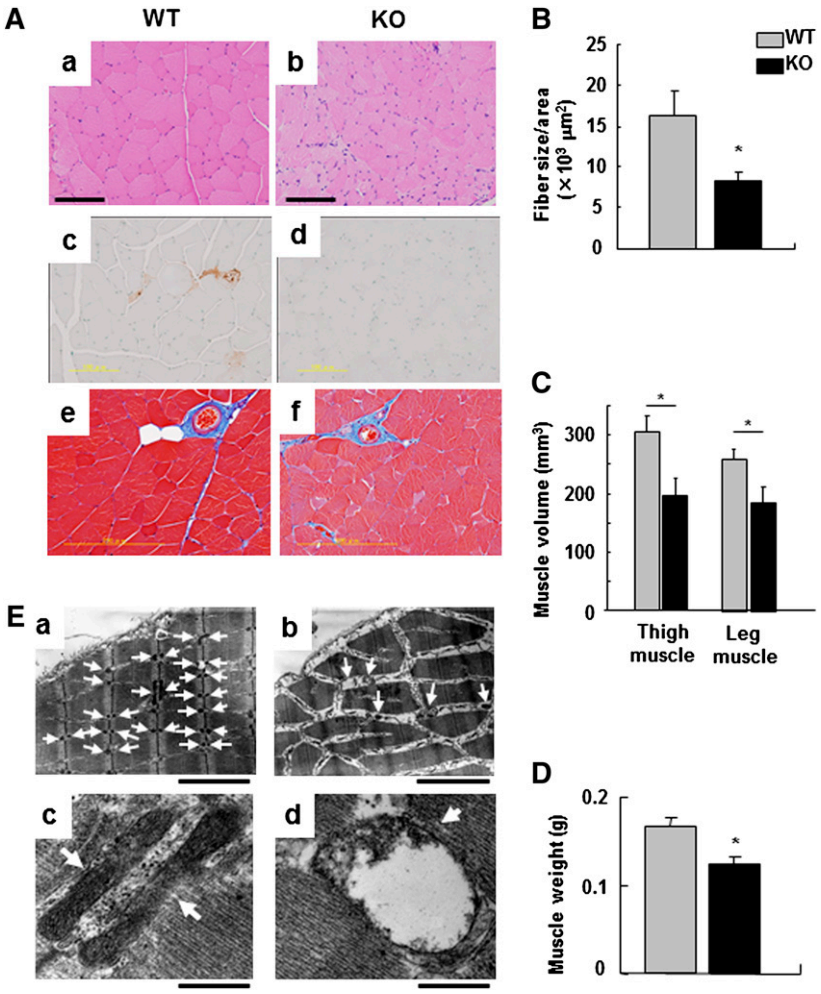

Fig. 2. Histological analysis of thigh muscle from iPLA$_2$γ-WT and -KO mice. A: Cross-sections of thigh muscle from WT (a) and KO (b) mice were stained with hematoxylin and eosin. TUNEL staining of thigh muscle from WT (c) and KO (d) mice. Masson trichrome staining of thigh muscle from WT (e) and KO (f) mice. Scale bar: 100 μm. B: Evaluation of the sizes of muscle fibers in iPLA$_2$γ-WT and -KO mice. Values are means ± SE (n = 3). C: Volumes of thigh and leg muscles in iPLA$_2$γ-WT (gray bar) and -KO (black bar) mice at four months of age by using CT scan analysis. Quantitative data are means ± SE. * $P < 0.05$ versus WT (n = 6). D: Weights of thigh muscles in iPLA$_2$γ-WT (gray bar) and -KO (black bar) mice. Quantitative data are means ± SE. * $P < 0.05$ versus WT (n = 6). E: Electron microscopy of iPLA$_2$γ-WT and -KO skeletal muscles. Skeletal muscles from four-month-old WT [(a) and (c)] and KO [(b) and (d)] mice were fixed in 2.5% (v/v) glutaraldehyde in phosphate buffer, and then analyzed by transmission electron microscopy. The micrographs show abnormal mitochondria and myofiber degeneration in the muscle from KO mice compared with that of WT mice. Arrows show mitochondria. Scale bar, 1 μm [(a) and (b)] and 100 nm [(c) and (d)]. Abbreviations: CT, computed tomography; iPLA$_2$, calcium-independent PLA$_2$; KO, knockout; WT, wild-type.

mice than in their WT littermates (Fig. 2C). Furthermore, the thigh muscle was significantly lighter in iPLA$_2$γ-KO mice than in their WT littermates (Fig. 2D). However, neither TUNEL staining (Fig. 2A, c and d) nor Masson trichrome staining (Fig. 2A, e and f) provided increased signals in iPLA$_2$γ-KO mice relative to WT mice, indicating that the observed muscle phenotypes in the KO mice were not due to increased apoptosis and fibrosis, respectively, of muscle fibers. In addition, the mRNA expression of several inflammatory cytokines, including IL-1β, IL-6, and TNF-α (33–36), in iPLA$_2$γ-KO skeletal muscle was similar to that of WT mice (supplementary Fig. III), implying that the muscle atrophy in iPLA$_2$γ-KO mice was not accompanied by an inflammatory response.

We further performed transmission electron microscopic analysis of the skeletal muscle (Fig. 2E). Compared with four-month-old WT skeletal muscle, in which individual myofilaments were aligned regularly (Fig. 2E, a and c), the age-matched iPLA$_2$γ-KO muscle exhibited a reduction of mitochondrial number, increase of swollen mitochondria, and degeneration of myofilaments (Fig. 2E, b and d). In the KO mice, the mitochondria varied in size and many contained abnormal cristae (Fig. 2E, b and d). It was noteworthy that by electron microscopic examination, signs of myofilament degeneration as well as mitochondrial proliferation and swelling, typical features of mitochondrial stress, were observed in iPLA$_2$γ-KO mice even at one month of age (supplementary Fig. IIB, a-d). Thus, mitochondrial

stress had come out ahead of the onset of the muscle weakness in the KO mice.

We next assessed whether the observed muscle atrophy in iPLA$_2$γ-KO mice was caused by abnormal myogenic differentiation. The primary myoblastic cells prepared from the thigh muscle of iPLA$_2$γ-KO mice grew normally under high-FCS culture conditions. When placed under low-HS conditions, these cells were able to form myotubes normally, and the number of myotubes did not show any significant difference between WT and KO mice (supplementary Fig. IVA, B). On Western blot analysis, the expression of α-actinin, a microfilament protein that is necessary for the attachment of actin filaments to the Z-line membrane in muscle cells (37), was induced similarly in both WT- and iPLA$_2$γ-KO-derived myoblasts during the process of differentiation (after 3–6 days of culture) (supplementary Fig. IVC). These results suggest that the deficiency of iPLA$_2$γ does not affect myogenic differentiation per se.

Mitochondrial dysfunction and increased oxidative stress in iPLA$_2$γ-KO muscle

To further address the alterations in the mitochondria of iPLA$_2$γ-KO mice, the expression of several mitochondrial proteins in homogenates of thigh muscles from WT and iPLA$_2$γ-KO mice were examined by Western blotting. We found notable decreases in the expression levels of several mitochondrial markers, such as porin, F_1-ATPase, and SOD2 (Mn-SOD), in four-month-old iPLA$_2$γ-KO mice compared with WT mice (**Fig. 3A**), suggesting that the number and/or integrity of mitochondria was lower in iPLA$_2$γ-KO muscle than in WT muscle. Furthermore, the ATP level in homogenates of the skeletal muscle was lower in iPLA$_2$γ-KO mice than in WT mice (Fig. 3B), consistent with the reduction of F_1-ATPase, an essential component of mitochondrial ATP synthesis, in the KO mice.

Considering that mitochondria are the most important cellular source of reactive oxygen species (ROS), we next analyzed whether the skeletal muscle of iPLA$_2$γ-KO mice would be exposed to oxidative stress resulting from mitochondrial dysfunction. The level of lipid peroxidation, as indicated by the accumulation of MDA, was significantly higher in iPLA$_2$γ-KO muscle than in WT muscle (Fig. 3C). It has been shown that oxidative stress induces several enzymes involved in antioxidant defense to minimize oxidative damage (38–40). Q-PCR evaluation revealed that the expression levels of *Hmox1* (heme oxygenase-1), *Nqo1* (NAD(P)H dehydrogenase, quinine-1) and *Mt1* (metallothionein-1) were higher in the skeletal muscle of iPLA$_2$γ-KO mice than in that of WT mice (Fig. 3D). In addition, the mRNA level of *Fbxo32* (atrogin-1 or muscle atrophy F-box), which encodes a muscle-associated, ROS-inducible E3 ubiquitin ligase, was substantially higher in the iPLA$_2$γ-KO muscle (Fig. 3D).

To assess whether these phenotypes were caused directly by intrinsic mitochondrial defects or by the secondary effects of systemic growth abnormalities, we performed knockdown of iPLA$_2$γ by siRNA in C2C12 cells, a mouse myoblast cell line. As shown in Fig. 3E, the expression of endogenous iPLA$_2$γ was markedly reduced in cells transfected with iPLA$_2$γ siRNA (iPLA$_2$γ-KD) relative to those transfected with control siRNA (mock). The ATP content in the cell lysate was lower in iPLA$_2$γ-KD C2C12 cells than in mock cells (Fig. 3F). The accumulation of MDA was substantially higher in iPLA$_2$γ-KD cells than in mock cells (Fig. 3G). These results suggest that knockdown of iPLA$_2$γ in C2C12 cells also leads to mitochondrial dysfunction, accompanied by increased oxidative stress.

Alterations of phospholipid compositions in skeletal muscle by iPLA$_2$γ deficiency

In the previous studies, the content of CL, a phospholipid that is mostly confined to mitochondrial membranes, was changed in the heart and brain of iPLA$_2$γ-deficient mice (18, 19). We also investigated the phospholipid composition in the skeletal muscle from iPLA$_2$γ-KO mice compared with that from WT mice. TLC analysis demonstrated a statistically significant decrease in CL content in iPLA$_2$γ-deficient muscle compared with WT muscle (**Table 1**). The content of phosphatidylglycerol, a precursor of CL, in the skeletal muscle also showed a similar tendency of decrease in iPLA$_2$γ-KO mice compared with WT mice, whereas the differences in the contents of PC and PE were only subtle and not statistically significant between the genotypes (Table 1). To examine whether there would be some alterations in individual molecular species of PC and PE between iPLA$_2$γ-KO and WT muscles, we performed ESI/MS analyses of these phospholipids. Representative ESI/MS patterns of PC and PE species extracted from WT or iPLA$_2$γ-KO muscles are shown in **Fig. 4A** and C, respectively. Significant reductions in some molecular species were observed in the KO mice compared with WT mice. Four independent trials of the ESI/MS analysis showed that PC subclasses with C34:2 (C16:0 and C18:2; m/z = 758.6) and C36:4 (C16:0 and C20:4, m/z = 782.6) (Fig. 4B) and PE subclasses with C38:6 (C16:0 and C22:6, m/z = 764.5) and C40:7 (C18:1 and C22:6, m/z = 790.5) (Fig. 4D) were significantly reduced in iPLA$_2$γ-KO mice compared with WT mice. Phosphatidylinositol and phosphatidylserine did not show any significant difference between WT and iPLA$_2$γ-KO mice (data not shown).

Alterations of prostanoid contents in skeletal muscle by iPLA$_2$γ deficiency

As described above, we previously demonstrated that iPLA$_2$γ has a regulatory role in AA release and eicosanoid generation in vitro (20). As it has been reported that some prostanoids have myoprotective activities (41, 42), we here quantified the contents of PGE_2, 6-keto$PGF_{1\alpha}$, PGD_2, $PGF_{2\alpha}$, and TXB_2 in homogenates of the skeletal muscles from WT and iPLA$_2$γ-KO mice. In the skeletal muscle of WT mice, PGE_2 and 6-keto$PGF_{1\alpha}$ were much more abundant than $PGF_{2\alpha}$, PGD_2, and TXB_2 (**Fig. 5A**). Among these prostanoids, the levels of PGD_2 and $PGF_{2\alpha}$ were significantly lower in iPLA$_2$γ-KO skeletal muscle than in WT skeletal muscle, although the 6-keto$PGF_{1\alpha}$, PGE_2 and TXB_2 levels did not differ appreciably between the genotypes (Fig. 5A). Furthermore, the reduction of some, if not all, prostanoids in the KO mice was not limited to the skeletal muscle, as the levels of $PGF_{2\alpha}$, PGD_2, and TXB_2 but not of the

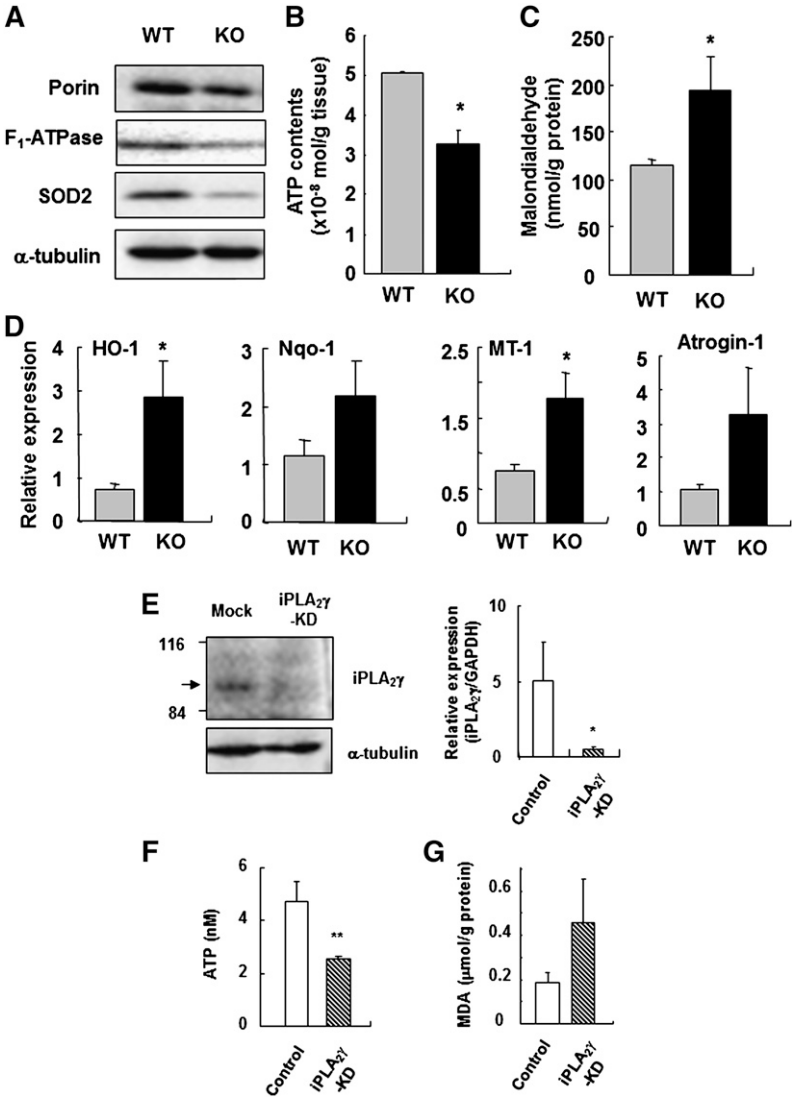

Fig. 3. Mitochondrial dysfunction and increased lipid peroxidation by lacking of $iPLA_2\gamma$ expression. A: Western blot analysis of mitochondrial markers in $iPLA_2\gamma$-WT and -KO muscles at four months of age. A blot for α-tubulin was used as a loading control. B: ATP contents in skeletal muscles from WT (gray bar) and KO mice (black bar) (n = 3). Quantitative data are means ± SE. *, $P < 0.05$ versus WT. *C,* lipid peroxidation assay of skeletal muscles in WT (gray bar) and KO mice (black bar) (n = 7). Quantitative data are means ± SE. *, $P < 0.05$ versus WT. *D,* Q-PCR analysis of the mRNA expression for antioxidant-defense enzymes in skeletal muscles from WT (gray bar) and KO mice (black bar) (n = 6-7). Quantitative data are means ± SE. *$P < 0.05$ versus WT. E: Reduction in $iPLA_2\gamma$ protein (left) and mRNA (right) expression after transfection of the C2C12 myoblast cells. Quantitative data are means ± SE. *$P < 0.05$ versus WT (n = 3). F: ATP contents in control (white bar) and $iPLA_2\gamma$-KD C2C12 cells (striped bar). Quantitative data are means ± SE. **$P < 0.01$ versus control (n = 3). G: Lipid peroxidation assay of control (white bar) and $iPLA_2\gamma$-KD C2C12 cells (striped bar) (n = 5). Quantitative data are means ± SE. *$P < 0.05$ versus WT. Abbreviations: CT, computed tomography; $iPLA_2$, calcium-independent PLA_2; KO, knockout; Q-PCR, quantitative RT-PCR; WT, wild-type.

major prostanoids PGE_2 and 6-ketoPGF$_{1\alpha}$ in the heart were also significantly reduced by $iPLA_2\gamma$ deficiency (Fig. 5B).

DISCUSSION

We found that genetic deletion of $iPLA_2\gamma$ in mice led to muscle atrophy and weakness. These findings could provide, at least in part, an explanation for the growth retardation, kyphosis, scoliosis, and reduced exercise capacity of the null mice. The muscle atrophy in $iPLA_2\gamma$-KO mice was accompanied by mitochondrial degeneration, decreased CL and ATP levels, and elevated lipid peroxidation. These results are compatible with recent studies using another line of $iPLA_2\gamma$-KO mice, in which impaired energy expenditure and oxygen consumption occurred in the brown adipose tissue, heart, and brain, most probably because of compromised mitochondrial CL homeostasis (18, 19). Furthermore, we found that the contents of $PGF_{2\alpha}$ and PGD_2 were significantly decreased in $iPLA_2\gamma$-KO muscle compared with WT muscle. The latter finding is, to the best of our knowledge, the first demonstration that the absence of $iPLA_2\gamma$ is linked to reduced biosynthesis of lipid mediators in vivo.

In eukaryotes, CL is present exclusively in the membranes of mitochondria, where it interacts with a number

TABLE 1. Phospholipid compositions in skeletal muscle by TLC analysis

Genotype	Phospholipid Class			
	CL	PE	PC	Phosphatidylglycerol
	Mean ± SEM (%)			
WT	1.89 ± 0.28	12.57 ± 2.67	34.25 ± 8.9	5.33 ± 2.44
KO	0.96 ± 0.21[a]	11.08 ± 1.62	29.64 ± 4.71	1.75 ± 0.47

Total lipids were extracted from homogenates of thigh muscle from $iPLA_2\gamma^{+/+}$ (WT) and $iPLA_2\gamma^{-/-}$ (KO) mice and separated on TLC silica gel plates. The TLC plates were stained by iodine vapor to visualize the phospholipids. After scraping the silica in bands of PC, PE, CL, and phosphatidylglycerol from the plates, the lipids were extracted from the silica two times with the method of Bligh and Dyer (25). Individual phospholipids were quantified by a molybdenum blue method. Quantitative data are means ± SE. CL, cardiolipin; PC, phosphatidylcholine; PE, phosphatidylethanolamine; $iPLA_2$, calcium-independent PLA_2; KO, knockout; WT, wild-type.

[a]$P < 0.05$ versus WT (n = 6).

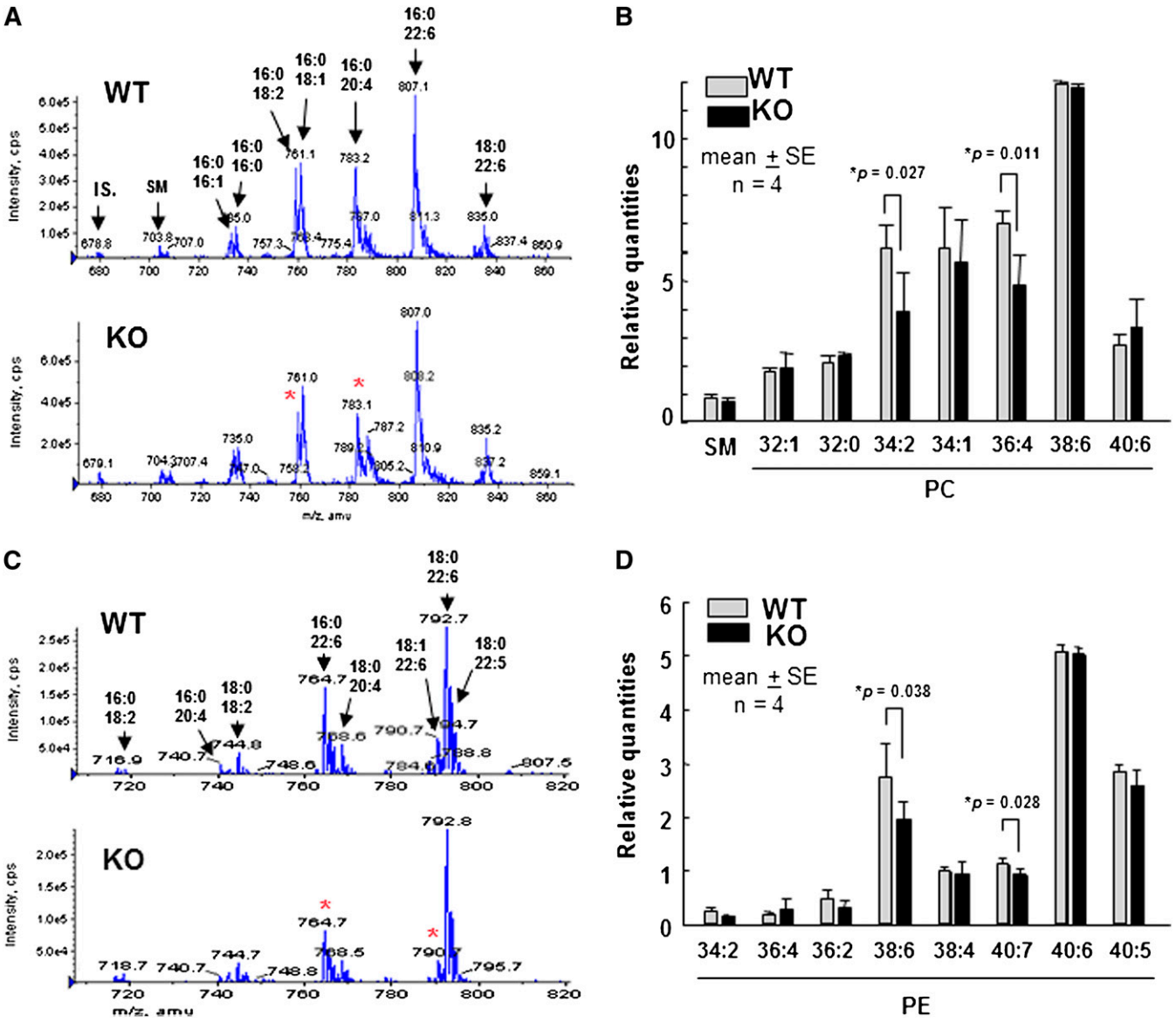

Fig. 4. ESI/MS analysis of PC and PE species in iPLA$_2$γ-WT and -KO skeletal muscles. Total lipids were extracted from thigh muscle homogenates and then subjected to ESI/MS analysis of PC (A and B) and PE (C and D). Representative ESI/MS profile (A and C) and quantitative results of four independent experiments. Means ± SE. *$P < 0.05$ versus control (n = 4) are shown in (B) and (D). Asterisks in (A) and (B) show altered molecular species. Abbreviations: IS, internal standard; PC, phosphatidylcholine; PE, phosphatidylethanolamine; iPLA$_2$, calcium-independent PLA$_2$; KO, knockout; SM, sphingomyelin; WT, wild-type.

of mitochondrial proteins and is essential for optimal mitochondrial functions (43–46). CL is synthesized de novo through condensation of phosphatidylglycerol with cytidine diphosphate-diacylglycerol (CDP-DAG) catalyzed by cardiolipin synthase (CLS). Following its biosynthesis, CL is actively remodeled to achieve its final acyl composition specific for cells and tissues. An important CL remodeling enzyme is tafazzin, a CL transacylase. Mutations in the tafazzin gene cause the X-linked recessive disorder Barth syndrome, which presents with dilated cardiomyopathy, skeletal myopathy, cyclic neutropenia, and growth retardation. Tafazzin-mediated transacylation of CL is particularly important in the heart and skeletal muscle, in which ~80% of CL molecules are remodeled to be tetralinoleoyl-CL (47). Defective tafazzin function results in reduced reacylation of monolyso-CL and eventually in deficiency of CL (48–51); accordingly, patients with Barth syndrome present symptoms, such as cardioskeletal myopathy and exercise intolerance, which are commonly associated with mitochondrial diseases (52). It was very recently shown that genetic inactivation of the iPLA$_2$β ortholog in *Drosophila* suppressed the phenotype caused by tafazzin deficiency (53). These findings suggested that iPLA$_2$β or its related paralog(s) might be involved in the machinery of CL deacylation and remodeling in mammals. In this context, it is noteworthy that iPLA$_2$β-KO mice develop age-dependent neurological impairment (13, 54), and mutations in the human iPLA$_2$β gene (*PLA2G6*) have been identified in patients with infantile neuroaxonal dystrophy and neurodegeneration with iron accumulation in the brain (16, 55).

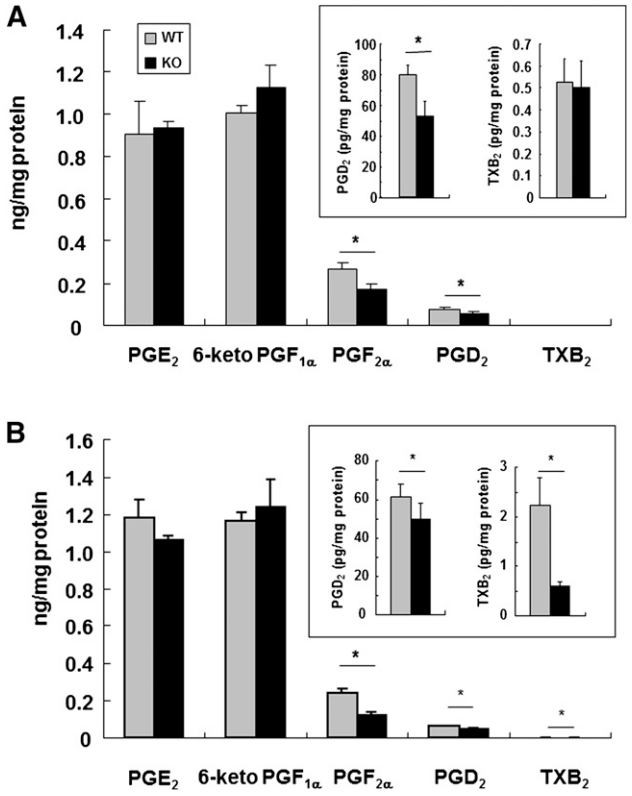

Fig. 5. Prostanoid contents in skeletal muscle and heart. Contents of PGE_2, 6-keto$PGF_{1\alpha}$ (a stable metabolite of PGI_2), $PGF_{2\alpha}$, PGD_2, and TXB_2 (a stable metabolite of TXA_2) in homogenates of skeletal muscle (A) and heart (B) were quantified by enzyme immunoassay kits. Quantitative data are means ± SE. $^*P < 0.05$ versus control (n = 3–7). Abbreviations: KO, knockout; PGE_2, prostaglandin E_2; PGI_2, prostaglandin I_2; TXA_2, thromboxane A_2; WT, wild-type.

However, there have been no reports demonstrating that iPLA$_2$β-KO mice display cardioskeletal myopathy, exercise intolerance, and growth retardation, which are typical symptoms of mitochondrial diseases, including Barth syndrome. On the other hand, here we have demonstrated that iPLA$_2$γ-KO mice showed age-dependent growth retardation and skeletal muscle loss, and that in these mice, mitochondrial degeneration and dysfunction preceded. The dramatic reduction of CL and its precursor phosphatidylglycerol in iPLA$_2$γ-KO muscle compared with WT muscle further supports the impaired CL remodeling, which may lead to mitochondrial degeneration and thereby reduced ATP synthesis in iPLA$_2$γ-KO mice. It has been reported that another line of iPLA$_2$γ-KO mice also harbored myocardial and neuronal phenotypes with altered CL contents (18, 19). Moreover, neurodegeneration occurred at a much earlier stage in iPLA$_2$γ-KO mice (19) than in iPLA$_2$β-KO mice (13). Thus, in mice, iPLA$_2$γ may cooperate with the transacylase tafazzin to control the remodeling of CL and thereby maintain homeostasis of mitochondria in tissues with high energy expenditure and high oxygen consumption (i.e., cardiac and skeletal muscles) under physiological conditions.

Mitochondria are the most important cellular source of ROS. If not adequately neutralized, ROS can damage cells by peroxidation of membrane phospholipids. In the present study, the loss of iPLA$_2$γ resulted in increased lipid peroxidation in the skeletal muscle. Likewise, the knockdown of iPLA$_2$γ in C2C12 myoblastic cells also caused elevation of lipid peroxidation and reduction of ATP synthesis, thus mirroring the in vivo effects of iPLA$_2$γ deficiency. Kinsey et al. (56) have also reported that the knockdown of iPLA$_2$γ expression in the primary cultures of rabbit renal proximal tubule cells induced elevation of lipid peroxidation and decrease in mitochondrial functions. Our ESI/MS analyses of phospholipids in iPLA$_2$γ-KO and WT muscles revealed that some PE and PC molecular species containing linoleic acid, AA, and docosahexaenoic acid were decreased in iPLA$_2$γ-KO muscle. As phospholipids bearing polyunsaturated fatty acids are particularly susceptible to peroxidation, these decreases may reflect the occurrence of oxidative modification of membranes. Among mitochondrial phospholipids, CL is regarded as a target of ROS attack, because it is particularly rich in linoleic acid and localizes in the inner mitochondrial membrane near the ROS-producing sites. Furthermore, peroxidation of CL in mitochondria has been suggested to initiate the mitochondria-mediated apoptotic signal (57). Thus, cells must replace peroxidized fatty acyl residues in phospholipids with native fatty acids by a sequential action of PLA_2 and acyltransferase to keep mitochondrial membranes in an optimal state. From this point of view, iPLA$_2$γ may be responsible for the repair of peroxidized CL in mitochondria. It has been proposed that the consecutive action of PLA_2 and glutathione peroxidase (GPx) is required to reduce lipid peroxides in mitochondria (24). Like the gene disruption of iPLA$_2$γ observed in the present study, gene disruption of cGPx, one of the GPx isozymes, has also been shown to result in growth retardation, presumably due in part to mitochondria disorders (58). Thus, iPLA$_2$γ may play a role in removing peroxidized CL from the mitochondrial membrane, thereby preserving membrane integrity.

Oxidative stress induces the expression of antioxidant genes that protect against oxidative stress (59–61). In further support of the idea that oxidative stress is increased by the absence of iPLA$_2$γ, we found that the mRNA levels of several antioxidant genes, including *Hmox1*, *Nqo1*, *Mt1,* and *Fbxo32*, were increased in iPLA$_2$γ-KO muscle compared with WT muscle. These results suggest that, in the iPLA$_2$γ-KO muscle, a set of antioxidant genes was induced in response to ROS following mitochondrial damage. *Hmox1* and *Nqo1* are induced through ROS-mediated activation of the transcription factor Nrf2 (60). Atrogin-1 (Fbxo32), an E3 ubiquitin ligase specifically expressed in cardiac and skeletal muscles, is dramatically upregulated by ROS in multiple atrophy models, as is muscle ring finger 1 (MuRF1), another E3 ubiquitin ligase (61–63). The increase in E3 ubiquitin ligases may facilitate ubiquitin/proteosome-dependent protein degradation, thereby contributing to muscular degeneration and atrophy. We further found that mRNA levels of iPLA$_2$β and cPLA$_2$α were increased in the iPLA$_2$γ-KO muscle. Previous studies have shown that oxidative stress induced by exogenous adding

of hydrogen peroxide or superoxide anion in macrophage cultures significantly increased $iPLA_2$ and $cPLA_2$ activities (64). It has been also shown that $iPLA_2\beta$ has an ability to repair oxidative modifications of mitochondrial lipids (65). In the $iPLA_2\gamma$-KO muscle, oxidative stress may induce the expression of $iPLA_2\beta$ and $cPLA_2\alpha$ as antioxidant genes.

In our previous report, overexpression of $iPLA_2\gamma$ was shown to facilitate cellular release of AA, which was converted to PGE_2 with preferred COX-1 coupling (20). Studies of eicosanoid contents in the skeletal muscle indicated that $PGF_{2\alpha}$ and PGD_2 were noticeably reduced in $iPLA_2\gamma$-KO muscle. Several PGs, such as PGE_2, $PGF_{2\alpha}$, PGI_2, and PGD_2, have been shown to be increased in the damaged muscle tissue, where they exhibit muscle repair functions (41). $PGF_{2\alpha}$ is produced by myoblasts and signals via the PGF receptor (FP) to increase myotube size by preventing myoblast apoptosis and by promoting muscular cell fusion and protein synthesis (42). Although the role of PGD_2 in muscular cells is controversial, it appears to play both beneficial and detrimental roles. Tokudome et al. reported that PGD_2 synthesis was protective against myocardial injury (66). In addition, 15-deoxy-delta-12, 14-PGJ_2 (15d-PGJ_2), a spontaneous dehydration product of PGD_2, has the ability to affect ROS generation by covalently modifying cellular proteins, such as NF-κB, to activate peroxisome proliferator activating receptor γ (PPARγ) as a ligand (67) and to block myotube formation in a PPARγ-independent manner (68). Thus, besides the regulation of mitochondrial membrane homeostasis, $iPLA_2\gamma$ may protect the muscle from damages by regulating the production of these prostanoids.

It was noteworthy that in the $iPLA_2\gamma$-KO mice, the production of major prostanoids, PGE_2 and PGI_2, was not affected, and only the synthesis of particular classes of prostanoid was suppressed. These results indicated that total AA supply from membrane phospholipids was not changed in the KO mice. AA from membrane phospholipids by $iPLA_2\gamma$ might be supplied specifically to particular downstream PG-biosynthetic enzymes (COXs and terminal PG synthases). It has been found that the biosynthesis of individual prostanoids shows distinct utilization of the two COX isoforms COX-1 and COX-2, probably because of the distinct functional coupling between COXs and terminal PG synthases (69). Interestingly, prostanoids that were affected by $iPLA_2\gamma$ deficiency (PGD_2, $PGF_{2\alpha}$, and TXA_2) in skeletal and cardiac muscles can be produced through COX-1 (69). $iPLA_2\gamma$ might be functionally coupled with COX-1 in preference to COX-2. However, even if AA supply accounts for the coupling of $iPLA_2\gamma$ with prostanoid synthesis, it still remains unclear how mitochondrial $iPLA_2\gamma$ could be coupled with COX enzymes that reside in the endoplasmic reticulum and nuclear envelope (70). In this regard, recent evidence suggests the presence of a mitochondria-endoplasmic reticulum tethering complex that connects inter-organelle calcium and lipid exchange (71). Alternatively, we could not rule out the possibility that the increased oxidative stress signaling in $iPLA_2\gamma$-KO muscle might secondarily downregulate other PLA_2, which in turn could supply AA to the $PGF_{2\alpha}$ and PGD_2-biosynthetic pathways, although $cPLA_2\alpha$ and $iPLA_2\beta$ were upregulated in the $iPLA_2\gamma$-KO muscle. Further details of the signaling role of $iPLA_2\gamma$, together with its mechanistic insights, need to be clarified in a future study.

Professor Ichiro Kudo died April 27, 2008. We greatly miss him as a scientist and friend. We offer sincere thanks to all friends, colleagues, and former collaborators of Prof. Kudo who showed him kindness during his lifetime.

REFERENCES

1. Kudo, I., and M. Murakami. 2002. Phospholipase A_2 enzymes. *Prostaglandins Other Lipid Mediat.* **68–69:** 3–58.
2. Murakami, M., and I. Kudo. 2001. Diversity and regulatory functions of mammalian secretory phospholipase A_2s. *Adv. Immunol.* **77:** 163–194.
3. Burke, J. E., and E. A. Dennis. 2009. Phospholipase A_2 structure/function, mechanism, and signaling. *J. Lipid Res.* **50:** S237–S242.
4. Jenkins, C. M., D. J. Mancuso, W. Yan, H. F. Sims, B. Gibson, and R. W. Gross. 2004. Identification, cloning, expression, and purification of three novel human calcium-independent phospholipase A_2 family members possessing triacylglycerol lipase and acylglycerol transacylase activities. *J. Biol. Chem.* **279:** 48968–48975.
5. Ackermann, E. J., E. S. Kempner, and E. A. Dennis. 1994. Ca^{2+}-independent cytosolic phospholipase A_2 from macrophage-like P388D1 cells. Isolation and characterization. *J. Biol. Chem.* **269:** 9227–9233.
6. Wolf, M. J., and R. W. Gross. 1996b. Expression, purification, and kinetic characterization of a recombinant 80-kDa intracellular calcium-independent phospholipase A_2. *J. Biol. Chem.* **271:** 30879–30885.
7. Balsinde, J., M. A. Balboa, and E. A. Dennis. 1997. Antisense inhibition of group VI Ca^{2+}-independent phospholipase A_2 blocks phospholipid fatty acid remodeling in murine P388D1 macrophages. *J. Biol. Chem.* **272:** 29317–29321.
8. Wolf, M. J., J. Wang, J. Turk, and R. W. Gross. 1997. Depletion of intracellular calcium stores activates smooth muscle cell calcium-independent phospholipase A_2. A novel mechanism underlying arachidonic acid mobilization. *J. Biol. Chem.* **272:** 1522–1526.
9. Roshak, A. K., E. A. Capper, C. Stevenson, C. Eichman, and L. A. Marshall. 2000. Human calcium-independent phospholipase A_2 mediates lymphocyte proliferation. *J. Biol. Chem.* **275:** 35692–35698.
10. Atsumi, G., M. Murakami, K. Kojima, A. Hadano, M. Tajima, and I. Kudo. 2000. Distinct roles of two intracellular phospholipase A_2s in fatty acid release in the cell death pathway. Proteolytic fragment of type IVA cytosolic phospholipase $A_2\alpha$ inhibits stimulus-induced arachidonate release, whereas that of type VI Ca^{2+}-independent phospholipase A_2 augments spontaneous fatty acid release. *J. Biol. Chem.* **275:** 18248–18258.
11. Smani, T., S. I. Zakharov, P. Csutora, E. Leno, E. S. Trepakova, and V. M. Bolotina. 2004. A novel mechanism for the store-operated calcium influx pathway. *Nat. Cell Biol.* **6:** 113–120.
12. Bao, S., A. Bohrer, S. Ramanadham, W. Jin, S. Zhang, and J. Turk. 2006. Effects of stable suppression of Group VIA phospholipase A_2 expression on phospholipid content and composition, insulin secretion, and proliferation of INS-1 insulinoma cells. *J. Biol. Chem.* **281:** 187–198.
13. Shinzawa, K., H. Sumi, M. Ikawa, Y. Matsuoka, M. Okabe, S. Sakoda, and Y. Tsujimoto. 2008. Neuroaxonal dystrophy caused by group VIA phospholipase A_2 deficiency in mice: a model of human neurodegenerative disease. *J. Neurosci.* **28:** 2212–2220.
14. Ramanadham, S., K. E. Yarasheski, M. J. Silva, M. Wohltmann, D. V. Novack, B. Christiansen, X. Tu, S. Zhang, X. Lei, and J. Turk. 2008. Age-related changes in bone morphology are accelerated in group VIA phospholipase A_2 ($iPLA_2\beta$)-mull mice. *Am. J. Pathol.* **172:** 868–881.
15. Bao, S., D. J. Miller, Z. Ma, M. Wohltmann, G. Eng, S. Ramanadham, K. Moley, and J. Turk. 2004. Male mice that do not express group VIA phospholipase A_2 produce spermatozoa with impaired motility and have greatly reduced fertility. *J. Biol. Chem.* **279:** 38194–38200.

16. Morgan, N. V., S. K. Westaway, J. E. Morton, A. Gregory, P. Gissen, S. Sonek, H. Cangul, J. Coryell, N. Canham, N. Nardocci, et al. 2006. PLA2G6, encoding a phospholipase A_2, is mutated in neurodegenerative disorders with high brain iron. *Nat. Genet.* **38:** 752–754.
17. Mancuso, D. J., C. M. Jenkins, and R. W. Gross. 2000. The genomic organization, complete mRNA sequence, cloning, and expression of a novel human intracellular membrane-associated calcium-independent phospholipase A_2. *J. Biol. Chem.* **275:** 9937–9945.
18. Mancuso, D. J., H. F. Sims, X. Han, C. M. Jenkins, S. P. Guan, K. Yang, S. H. Moon, T. Pietka, N. A. Abumrad, P. H. Schlesinger, et al. 2007. Genetic ablation of calcium-independent phospholipase $A_2\gamma$ leads to alterations in mitochondrial lipid metabolism and function resulting in a deficient mitochondrial bioenergetic phenotype. *J. Biol. Chem.* **282:** 34611–34622.
19. Mancuso, D. J., P. Kotzbauer, D. F. Wozniak, H. F. Sims, C. M. Jenkins, S. P. Guan, X. Han, K. Yang, G. Sun, I. Malik, et al. 2007. Genetic ablation of calcium-independent phospholipase $A_2\gamma$ leads to alterations in hippocampal cardiolipin content and molecular species distribution, mitochondrial degeneration, autophagy, and cognitive dysfunction. *J. Biol. Chem.* **284:** 35632–35644.
20. Murakami, M., S. Masuda, K. Ueda-Semmyo, E. Yoda, H. Kuwata, Y. Takanezawa, J. Aoki, H. Arai, H. Sumimoto, Y. Ishikawa, et al. 2005. Group VIB Ca^{2+}-independent phospholipase $A_2\gamma$ promotes cellular membrane hydrolysis and prostaglandin production in a manner distinct from other intracellular phospholipase A_2. *J. Biol. Chem.* **280:** 14028–14041.
21. Kuwata, H., C. Fujimoto, E. Yoda, S. Shimbara, Y. Nakatani, S. Hara, M. Murakami, and I. Kudo. 2007. A novel role of group VIB calcium-independent phospholipase A_2 (iPLA$_2\gamma$) in the inducible expression of group IIA secretory PLA_2 in rat fibroblastic cells. *J. Biol. Chem.* **282:** 20124–20132.
22. Yan, W., C. M. Jenkins, X. Han, D. J. Mancuso, H. F. Sims, K. Yang, and R. W. Gross. 2005. The highly selective production of 2-arachidonoyl lusophosphatidylcholine catalyzed by purified calcium-independent phospholipase $A_2\gamma$. *J. Biol. Chem.* **280:** 26669–26679.
23. Tanioka, T., Y. Nakatani, N. Semmyo, M. Murakami, and I. Kudo. 2000. Molecular identification of cytosolic prostaglandin E_2 synthase that is functionally coupled with cyclooxygenase-1 in immediate prostaglandin E_2 biosynthesis. *J. Biol. Chem.* **275:** 32775–32782.
24. Taniwaki, T., K. Haruna, H. Nakamura, T. Sekimoto, Y. Oike, T. Imaizumi, F. Saito, M. Muta, Y. Soejima, A. Utoh, et al. 2005. Characterization of an exchangeable gene trap using pU-17 carrying a stop codon-beta geo cassette. *Dev. Growth Differ.* **47:** 163–172.
25. Bligh, E. G., and W. J. Dyer. 1959. A rapid method of total lipid extraction and purification. *Can. J. Physiol. Pharmacol.* **37:** 911–917.
26. Rouser, G., A. N. Siakotos, and S. Fleischer. 1966. Quantitative analysis of phospholipids by thin-layer chromatography and phosphorus analysis of spots. *Lipids.* **1:** 85–86.
27. Kamei, D., K. Yamakawa, Y. Takegoshi, M. Mikami-Nakanishi, Y. Nakatani, S. Oh-Ishi, H. Yasui, Y. Azuma, N. Hirasawa, K. Ohuchi, et al. 2004. Reduced pain hypersensitivity and inflammation in mice lacking microsomal prostaglandin E synthase-1. *J. Biol. Chem.* **279:** 33684–33695.
28. Mancuso, D. J., C. M. Jenkins, H. F. Sims, J. M. Cohen, J. Yang, and R. W. Gross. 2004. Complex transcriptional and translational regulation of iPLA$_2\gamma$ resulting in multiple gene products containing dual competing sites for mitochondrial or peroxisomal localization. *Eur. J. Biochem.* **271:** 4709–4724.
29. Colvin, J. S., B. A. Bohne, G. W. Harding, D. G. McEwen, and D. M. Ornitz. 1996. Skeletal overgrowth and deafness in mice lacking fibroblast growth factor receptor 3. *Nat. Genet.* **12:** 390–397.
30. Tourtellotte, W. G., and J. Milbrandt. 1998. Sensory ataxia and muscle spindle agenesis in mice lacking the transcription factor Egr3. *Nat. Genet.* **20:** 87–91.
31. Dabovic, B., Y. Chen, C. Colarossi, H. Obata, L. Zambuto, M. A. Perle, and D. B. Rifkin. 2002. Bone abnormalities in latent TGF-β binding protein (Ltbp)-3-null mice indicate a role for Ltbp-3 in modulating TGF- β bioavailability. *J. Cell Biol.* **156:** 227–232.
32. Baribault, H., J. Danao, J. Gupte, L. Yang, B. Sun, W. Richards, and H. Tian. 2006. The G-protein-coupled receptor GPR103 regulates bone formation. *Mol. Cell. Biol.* **26:** 709–717.
33. Lang, N. P., M. S. Tonetti, J. Suter, J. Sorrell, G. W. Duff, and K. S. Kornman. 2000. Effect of interleukin-1 gene polymorphisms on gingival inflammation assessed by bleeding on probing in a periodontal maintenance population. *J. Periodontal Res.* **35:** 102–107.
34. Emery, P., and M. Salmon. 1991. The immune response. 2. Systemic mediators of inflammation. *Br. J. Hosp. Med.* **45:** 164–168.
35. Kishimoto, T., S. Akira, and T. Taga. 1992. Interleukin-6 and its receptor: a paradigm for cytokines. *Science.* **258:** 593–597.
36. Birkedal-Hansen, H. 1993. Role of cytokines and inflammatory mediators in tissue destruction. *J. Periodontal Res.* **28:** 500–510.
37. Sjöblom, B., A. Salmazo, and K. Djinovi -Carugo. 2008. α-actinin structure and regulation. *Cell. Mol. Life Sci.* **65:** 2688–2701.
38. Kang, Y. J. 2007. Antioxidant defense against anthracycline cardiotoxicity by metallothionein. *Cardiovasc. Toxicol.* **7:** 95–100.
39. Takahashi, T., H. Shimizu, H. Morimatsu, K. Inoue, R. Akagi, K. Morita, and S. Sassa. 2007. Heme oxygenase-1: a fundamental guardian against oxidative tissue injuries in acute inflammation. *Mini Rev. Med. Chem.* **7:** 745–753.
40. Jaiswal, A. K. 2000. Regulation of genes encoding NAD(P) H:quinone oxidoreductases. *Free Radic. Biol. Med.* **29:** 254–262.
41. Velica, P., and C. M. Bunce. 2008. Prostaglandins in muscle regeneration. *J. Muscle Res. Cell Motil.* **29:** 163–167.
42. Horsley, V., and G. K. Pavlath. 2003. Prostaglandin $F_{2\alpha}$ stimulates growth of skeletal muscle cells via an NFATC2-dependent pathway. *J. Cell Biol.* **161:** 111–118.
43. Schlame, M., D. Rua, and M. L. Greenberg. 2000. The biosynthesis and functional role of cardiolipin. *Prog. Lipid Res.* **39:** 257–288.
44. Li, G., S. Chen, M. N. Thompson, and M. L. Greenberg. 2007. New insights into the regulation of cardiolipin biosynthesis in yeast: implications for Barth syndrome. *Biochim. Biophys. Acta.* **1771:** 432–441.
45. Houtkooper, R. H., and F. M. Vaz. 2008. Cardiolipin, the heart of mitochondrial metabolism. *Cell. Mol. Life Sci.* **65:** 2493–2506.
46. Schlame, M. 2008. Cardiolipin synthesis for the assembly of bacterial and mitochondrial membranes. *J. Lipid Res.* **49:** 1607–1620.
47. Schlame, M., S. Shanske, S. Doty, T. König, T. Sculco, S. DiMauro, and T. J. Blanck. 1999. Microanalysis of cardiolipin in small biopsies including skeletal muscle from patients with mitochondrial disease. *J. Lipid Res.* **40:** 1585–1592.
48. Xu, Y., M. Condell, H. Plesken, I. Edelman-Novemsky, J. Ma, M. Ren, and M. Schlame. 2006. A Drosophila model of Barth syndrome. *Proc. Natl. Acad. Sci. USA.* **103:** 11584–11588.
49. Gu, Z., F. Valianpour, S. Chen, F. M. Vaz, G. A. Hakkaart, R. J. Wanders, and M. L. Greenberg. 2004. Aberrant cardiolipin metabolism in the yeast taz1 mutant: a model for Barth syndrome. *Mol. Microbiol.* **51:** 149–158.
50. Valianpour, F., R. J. Wanders, H. Overmars, P. Vreken, A. H. Van Gennip, F. Baas, B. Plecko, R. Santer, K. Becker, and P. G. Barth. 2002. Cardiolipin deficiency in X-linked cardioskeletal myopathy and neutropenia (Barth syndrome, MIM 302060): a study in cultured skin fibroblasts. *J. Pediatr.* **141:** 729–733.
51. Vreken, P., F. Valianpour, L. G. Nijtmans, L. A. Grivell, B. Plecko, R. J. Wanders, and P. G. Barth. 2000. Defective remodeling of cardiolipin and phosphatidylglycerol in Barth syndrome. *Biochem. Biophys. Res. Commun.* **279:** 378–382.
52. Barth, P. G., F. Valianpour, V. M. Bowen, J. Lam, M. Duran, F. M. Vaz, and R. J. Wanders. 2004. X-linked cardioskeletal myopathy and neutropenia (Barth syndrome): an update. *Am. J. Med. Genet. A.* **126A:** 349–354.
53. Malhotra, A., I. Edelman-Novemsky, Y. Xu, H. Plesken, J. Ma, M. Schlame, and M. Ren. 2009. Role of calcium-independent phospholipase A_2 in the pathogenesis of Barth syndrome. *Proc. Natl. Acad. Sci. USA.* **17:** 2337–2341.
54. Malik, I., J. Turk, D. J. Mancuso, L. Montier, M. Wohltmann, D. F. Wozniak, R. E. Schmidt, R. W. Gross, and P. T. Kotzbauer. 2008. Disrupted membrane homeostasis and accumulation of ubiquitinated proteins in a mouse model of infantile neuroaxonal dystrophy caused by PLA2G6 mutations. *Am. J. Pathol.* **172:** 406–416.
55. Khateeb, S., H. Flusser, R. Ofir, I. Shelef, G. Narkis, G. Vardi, Z. Shorer, R. Levy, A. Galil, K. Elbedour, et al. 2006. PLA2G6 mutation underlies infantile neuroaxonal dystrophy. *Am. J. Hum. Genet.* **79:** 942–948.
56. Kinsey, G. R., J. L. Blum, M. D. Covington, B. S. Cummings, J. McHowat, and R. G. Schnellmann. 2008. Decreased iPLA$_2\gamma$ expression induces lipid peroxidation and cell death and sensitizes cells to oxidant-induced apoptosis. *J. Lipid Res.* **49:** 1477–1487.
57. Gonzalvez, F., and E. Gottlieb. 2007. Cardiolipin: setting the beat of apoptosis. *Apoptosis.* **12:** 877–885.
58. Esposito, L. A., J. E. Kokoszka, K. G. Waymire, B. Cottrell, G. R. MacGregor, and D. C. Wallace. 2000. Mitochondrial oxidative stress in mice lacking the glutathione peroxidase-1 gene. *Free Radic. Biol. Med.* **28:** 754–766.

59. Nakagawa, Y. 2004. Initiation of apoptotic signal by the peroxidation of cardiolipin of mitochondria. *Ann. N. Y. Acad. Sci.* **1011:** 177–184.
60. Leung, L., M. Kwong, S. Hou, C. Lee, and J. Y. Chan. 2003. Deficiency of the Nrf1 and Nrf2 transcription factors results in early embryonic lethality and severe oxidative stress. *J. Biol. Chem.* **278:** 48021–48029.
61. Cao, P. R., H. J. Kim, and S. H. Lecker. 2005. Ubiquitin-protein ligases in muscle wasting. *Int. J. Biochem. Cell Biol.* **37:** 2088–2097.
62. Cai, D., J. D. Frantz, N. E. Tawa, Jr., P. A. Melendez, B. C. Oh, H. G. Lidov, P. O. Hasselgren, W. R. Frontera, J. Lee, D. J. Glass, et al. 2004. IKKβ/NF-kappaB activation causes severe muscle wasting in mice. *Cell.* **119:** 285–298.
63. Li, Y. P., Y. Chen, A. S. Li, and M. B. Reid. 2003. Hydrogen peroxide stimulates ubiquitin-conjugating activity and expression of genes for specific E2 and E3 proteins in skeletal muscle myotubes. *Am. J. Physiol. Cell Physiol.* **285:** C806–C812.
64. Martinez, J., and J. J. Moreno. 2001. Role of Ca^{2+}-independent phospholipase A_2 on arachidonic acid release induced by reactive oxygen species. *Arch. Biochem. Biophys.* **392:** 257–262.
65. Zhao, Z., X. Zhang, C. Zhao, J. Choi, J. Shi, K. Song, J. Turk, and Z. A. Ma. 2010. Protection of pancreatic β-cells by group VIA phospholipase A_2-mediated repair of mitochondrial membrane peroxidation. *Endocrinology.* **151:** 3038–3048.
66. Tokudome, S., M. Sano, K. Shinmura, T. Matsuhashi, S. Morizane, H. Moriyama, K. Tamaki, K. Hayashida, H. Nakanishi, N. Yoshikawa, et al. 2009. Glucocorticoid protects rodent hearts from ischemia/reperfusion injury by activating lipocalin-type prostaglandin D synthase-derived PGD_2 biosynthesis. *J. Clin. Invest.* **119:** 1477–1488.
67. Uchida, K., and T. Shibata. 2008. 15-Deoxy-delta (12, 14)-prostaglandin J_2: an electrophilic trigger of cellular responses. *Chem. Res. Toxicol.* **21:** 138–144.
68. Hunter, J. G., M. F. van Delft, R. A. Rachubinski, and J. P. Capone. 2001. Peroxisome proliferator-activated receptor γ ligands differentially modulate muscle cell differentiation and MyoD gene expression via peroxisome proliferator-activated receptor γ-dependent and -independent pathways. *J. Biol. Chem.* **276:** 38297–38306.
69. Ueno, N., Y. Takegoshi, D. Kamei, I. Kudo, and M. Murakami. 2005. Coupling between cyclooxygenases and terminal prostanoid synthases. *Biochem. Biophys. Res. Commun.* **338:** 70–76.
70. Morita, I., M. Schindler, M. K. Reiger, J. C. Otto, T. Hori, D. L. DeWitt, and W. L. Smith. 1995. Different intracellular locations for prostaglandin endoperoxide H synthase-1 and -2. *J. Biol. Chem.* **270:** 10902–10908.
71. Kornmann, B., E. Currie, S. R. Collins, M. Schuldiner, J. Nunnari, J. S. Weissman, and P. Walter. 2009. An ER-mitochondria tethering complex revealed by a synthetic biology screen. *Science.* **325:** 477–481.